Sol−Gel Synthesis and Spectroscopic Properties of Thick Nanocrystalline CdSe Films

V. Ptatschek,[†] B. Schreder,[§] K. Herz,[||] U. Hilbert,[||] W. Ossau,[||] G. Schottner,[‡] O. Rahäuser,[†] T. Bischof,[§] G. Lermann,[§] A. Materny,[§] W. Kiefer,[§] G. Bacher,[||] A. Forchel,[||] D. Su,[⊥] M. Giersig,[⊥] G. Müller,[†] and L. Spanhel*[,†]

Institut für Silicatchemie der Universität Würzburg, Röntgenring 10, 97070 Würzburg, Germany; Fraunhofer Institut für Silicatforschung, Neuner Platz 2, 97082 Würzburg, Germany; Institut für Physikalische Chemie der Universität Würzburg, Am Hubland, 97074 Würzburg, Germany; Hahn-Meitner-Institut Berlin GmbH, Glienicker Str. 100, 14109 Berlin, Germany; and Physikalisches Institut der Universität Würzburg, Am Hubland, 97074 Würzburg, Germany

Received: May 1, 1997; In Final Form: June 21, 1997[⊗]

Two novel metal alkoxide-derived routes were developed for the synthesis of nanocrystalline CdSe layers with quantum dot sizes between 1 and 4 nm. The first route, where cadmium ethoxy−acetate is reacted with bis(trimethylsilyl)selenium in the presence of aminopropyltriethoxysilane (AMEO), yields highly concentrated alcoholic 0.5 M sols for direct coatings. The second route allows to grow CdSe clusters by infiltrating the selenium precursor into Cd-enriched organosilicate gel layers. The resulting optically transparent films with thicknesses near 10 μm (obtained in a single-step coating) were characterized by steady-state optical absorption and photoluminescence spectroscopy, high-resolution electron microscopy (HRTEM), X-ray diffraction (XRD), resonance Raman, and time-resolved photoluminescence spectroscopy. The experimental data reveal the presence of nanocrystals exhibiting a tetrahedral shape. The quantum dot films are strongly fluorescing, with a quantum yield near 10%. The decay characteristics of the photoluminescence signal after pulsed excitation is discussed taking into account the splitting of the quantum dot ground state as well as the influence of surface states. Furthermore, a size-dependent shift of the Raman band, attributed to the longitudinal optical phonon of the consolidated CdSe clusters, could be observed. This shift is accompanied by a broadening of the corresponding Raman line width. Both effects, the size-dependent shift as well as the broadening of the Raman line width, indicate that phonon confinement is present for the clusters under consideration.

Introduction

II−VI semiconductor clusters represent a novel state of inorganic matter with size tunable electronic and photonic properties.[1] The basic spectroscopic research on these low-dimensional systems started one decade ago, focusing mainly on colloids of low concentration. New improved synthesis strategy allowed to extend this work to application oriented studies on transparent films composed of consolidated nanocrystallites. For example, bias modulated electron transfer in transparent nanoporous metal oxide electrodes,[2] size-tunable photoconductivity in CdS containing organic polymer films,[3] and the observation of electroluminescence in organic polymer layers combined with self-organized CdSe quantum dot arrays[4] have been reported recently.

In this paper, we describe two metal alkoxide-derived routes leading to thick layers containing CdSe quantum dots of different sizes. The first route exploits the potential of inorganic−organic matrix systems. The precursors of these hydride composites are organically modified silanes, and if combined with other inorganic network-forming metal alkoxides, they are suitable precursor systems for the sol−gel synthesis of organosilicate copolymers loaded with semiconductor quantum dots[5] or other active optical molecular compounds.[6] The second route addresses synthesis of transparent film samples from highly concentrated 0.5 M quantum dot sols. After giving an insight into some of the structural properties, we will discuss the optical quality of the sols and films from the both routes and compare it with the spectral data presented previously by other groups on CdSe wurtzite nanocrystals.[4,7−12]

Furthermore, we will discuss results obtained from time-resolved photoluminescence (PL) and Raman experiments on nanocrystalline CdSe films. Time-resolved PL experiments have been shown to be a powerful tool in order to analyze the dynamics of photoexcited carriers in CdSe nanostructures.[7−12] However, the interpretation of the multiexponential decay mostly observed in such experiments is still under discussion, taking into account intrinsic properties of the nanocrystallites[7,10,12] as well as surface effects.[9,11] On the other hand, Raman spectroscopy has proven to be a valuable tool for the investigation of the vibronic properties of low-dimensional semiconductors.[13] However, inconsistent results were reported concerning the phonon confinement in CdSe and CdS clusters. Theoretical treatments of the phonon confinement predict a shift of the 1LO frequency to lower energies and an asymmetrical band broadening with decreasing cluster size.[13d,14] Besides line broadening, no remarkable frequency shift was reported for CdS or CdSe dots. This was explained in terms of a blue shift caused by strain effects on the cluster surface.[15] A further confinement effect is the appearance of surface optical (SO) modes, whose significance should rise with the increase of the surface-to-volume ratio. In this paper we discuss the size dependence of the line position, width, and shape of the 1LO Raman lines. The results are compared with predictions made by theoretical models concerned with the phonon confinement.

Experimental Section

General Synthesis. All reactions were carried out under argon using the Schlenk technique. Cadmium acetate dihydrate

[†] Institut für Silicatchemie der Universität Würzburg.
[‡] Fraunhofer Institut für Silicatforschung.
[§] Institut für Physikalische Chemie der Universität Würzburg.
[⊥] Hahn-Meitner-Institut Berlin GmbH.
[||] Physikalisches Institut der Universität Würzburg.
* Corresponding author: E-mail: spanhel@silchem.uni-wuerzburg.de.
[⊗] Abstract published in *Advance ACS Abstracts,* October 1, 1997.

S1089-5647(97)01487-9 CCC: $14.00

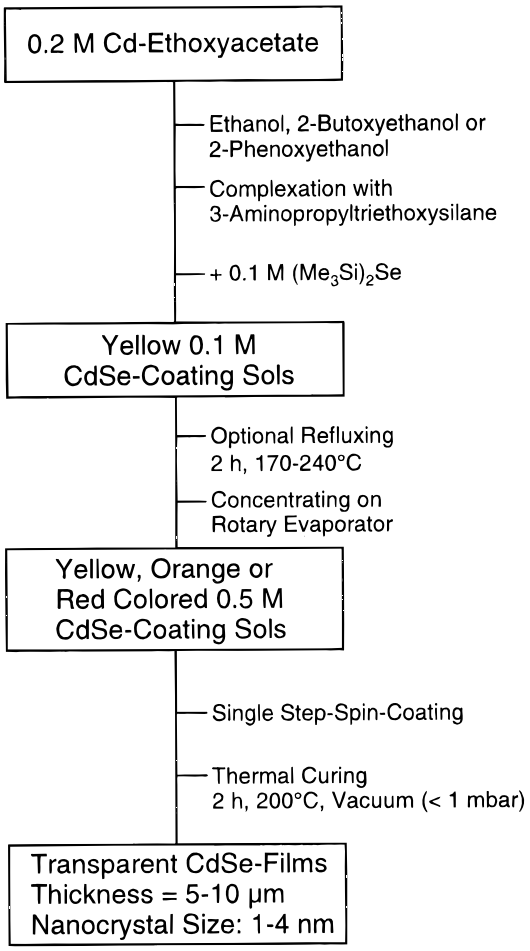

Figure 1. Flow diagram for the synthesis of AMEO-ordered nanocrystalline CdSe layers.

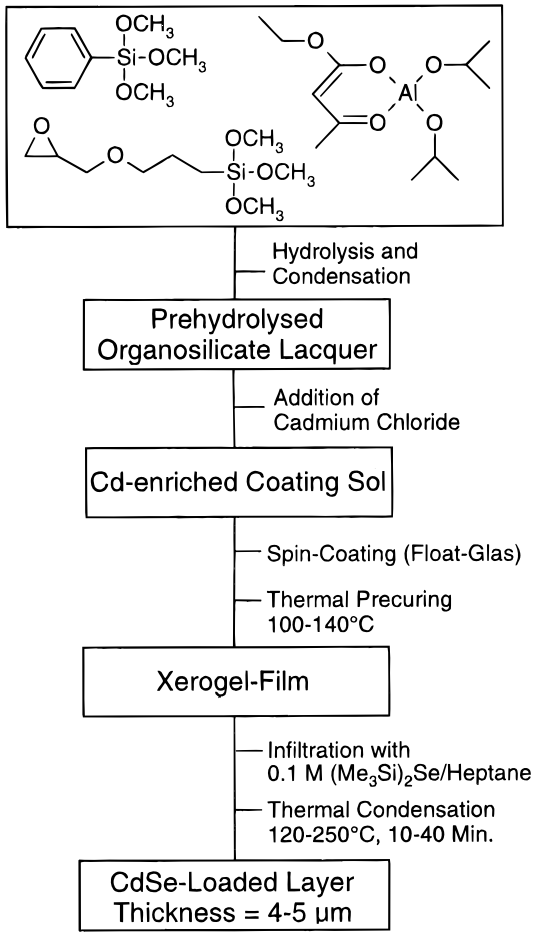

Figure 2. Flow diagram for the synthesis of organosilicate layers with encapsulated CdSe quantum dots.

(97%, Fluka), cadmium chloride (99.99%, Aldrich), bis(trimethylsilyl)selenium $(TMS)_2Se$ (98%, Acros), 3-aminopropyltriethoxysilane (AMEO) (98.5%, ABCR), 3-glycidoxypropyltrimethoxysilane (GLYMO) (98%, ABCR), phenyltrimethoxysilane (99%, ABCR), titanium *n*-butoxide (97%, ABCR), and aluminum diisopropoxide acetacetic ester chelate (Alfa) were used as received. Heptane, 2-butoxyethanol, and 2-phenoxyethanol were used as purchased from Aldrich.

AMEO-Capped CdSe Layers. Figure 1 shows a schematic flow diagram of the synthesis employed to prepare matrix-free CdSe layers composed of AMEO-capped CdSe quantum dots. In the first step, cadmium acetate dihydrate powder was suspended in ethanol and refluxed for 3 h, yielding a 0.1 M Cd precursor stock solution. The product of this starting step is a rather complex oligomerized cadmium ethoxy−acetate cluster as proved by FTIR and chemical elemental analysis.

For the subsequent CdSe cluster synthesis, 20 mL (2 mmol of Cd) of the precursor solution was evaporated under reduced pressure (0.1 mbar). The resulting dry residue was dissolved in 7.5 mL of ethanol, 2-butoxyethanol, or 2-phenoxyethanol on the addition of 2.21 g (10 mmol) of AMEO. The precomplexed colorless solutions were refluxed for 10 min and reacted under argon atmosphere with 225 mg (1 mmol) of $(TMS)_2Se$. The dropwise addition of this selenium source at room temperature produced 0.1 M CdSe solutions (ligand:Cd:Se = 5:2:1) containing 1.6 nm clusters (the gyration size was determined in SAXS measurements[18]) and 100% Cd^{2+} in excess. Under these starting concentration conditions, sharpest excitonic bands were seen in the corresponding optical absorption spectra of the produced yellowish sols (see Results and Discussion). Larger clusters sizes were obtained by refluxing yellow 2-butoxyethanolic and 2-phenoxyethanolic CdSe solutions for 2 h, resulting in orange (3.0 nm) or red (3.5 nm) sols, respectively. Optionally, the solvents and the excess of AMEO were subsequently removed under reduced pressure (0.1 mbar) to yield coating molarities up to 0.5 M.

In the last step, dust-free CdSe solutions with concentrations between 0.1 and 0.5 M were directly used to coat precleaned glass slides via a spin-on technique. The conditions of the drying and hardening depended on the boiling point of the coating solution. Layers from ethanolic CdSe−sols were heated for 1 h at 100 °C whereas 2 h at 250 °C under vacuum (<1 mbar) was needed to cure layers from 2-butoxyethanolic samples. CdSe layers from 2-phenoxyethanolic solutions were hardened for 2 h at 350 °C under vacuum (<1 mbar). Using the above-described procedure, optically transparent crack-free nanocrystalline layers with thicknesses near 10 μm were obtained.

CdSe Growth in Organosilicate Layers. The synthesis of CdSe-containing organosilicate composite layers is summarized in Figure 2. The matrix precursor was prepared by adding 3.06 g (9 mmol) of titanium *n*-butoxide to a mixture of 9.92 g (42 mmol) of GLYMO and 1.78 g (9 mmol) of phenyltrimethoxysilane. Thereafter, the hydrolysis was induced by dropping slowly 3.4 g (189 mmol) of purified water, and the reaction vessel was held under stirring for 2 h at temperatures between 5 and 15 °C. Alternatively, for the preparation of the Al lacquer, 2.47 g (9 mmol) of aluminum diisopropoxide acetacetic ester chelate was used instead of the titanium *n*-butoxide, and the reaction mixture was hydrolyzed with 3.08 g (171 mmol) of water. In the resulting lacquers, up to 0.4 M cadmium chloride

could be dissolved, exploiting the complexing power of the silanol-enriched noncondensed organosilicate ($2Si-OH + CdCl_2 \rightarrow -Si-O-Cd-O-Si + 2HCl$).

The layers were made up by spreading the Cd−copolymer solution on commercial glass slides via the spin-on technique. Finally, the wet films were precured at 100 °C for 1 min followed by reactive infiltration of a 0.1 M $(TMS)_2Se$/heptane solution. During this process, the color of the layers changed to yellow, indicating CdSe formation. The final condensation step via thermal treatment of the selenium-infiltrated layers at temperatures between 120 and 250 °C forces the initially generated small clusters to aggregate and fuse together. Transparent films with CdSe clusters of different size were formed in this way. The film thickness could be varied between 1 and 10 μm per single step coating by adjusting the viscosity of the honeylike lacquers by ethanol dilution.

Optical Characterization. Optical absorption spectra of the CdSe layers were collected at room temperature with a Hitachi U 3000 UV/vis spectrophotometer. Steady-state fluorescence spectra were taken with a Perkin-Elmer LS50 spectrofluorimeter. For the measurements of the 0.1−0.5 M CdSe solutions, 10 μm quartz cells were used. The thickness of the layers was measured with a Tencor-Alpha-Step-200 profilometer.

Time-Resolved Photoluminescence. In order to study the carrier dynamics in nanocrystalline CdSe films, time-resolved photoluminescence (PL) spectroscopy is used. For the fast decaying luminescence components, the sample excitation was performed by a pulsed, frequency-doubled titanium−sapphire laser, yielding optical pulses with a pulse length of 1.5 ps and a repetition rate of about 82 MHz. The excitation wavelength can be tuned between 420 and 500 nm. Typical excitation densities of 3 W/cm^2 were used in the experiments. The photoluminescence signal was dispersed by a 0.32 m Jobin-Yvon monochromator and recorded using a Streak camera system with a S20 cathode and a subsequent CCD camera. The overall time resolution of the setup is about 5 ps. For the time-resolved measurements on the slow decaying processes an argon ion laser was modulated by an acoustooptic modulator, and the signal was detected by a gated photon counter. All time-resolved PL measurements have been performed by using a LHe cryostate from 1.7 K up to room temperature.

Raman Spectroscopy. For details of the experimental setup we refer to ref 16. In short, the Raman spectra were recorded using a micro-Raman setup. For excitation, we used different emission lines of an argon ion laser. For detection the scanning multichannel technique was applied.[17] The scattered light was analyzed by means of a double monochromator (Spex Model 1404) which was equipped with a CCD camera (Photometrics Model RDS 2000). For the different cluster sizes, the excitation wavelength was chosen to be either resonant or at least near resonant with the lowest electronic transition of the semiconductor nanocrystallites ($1S_e-1S_h$ transition). In the case of the 1.6 nm as well as the 3.0 nm clusters, the Raman spectra were recorded with an excitation wavelength of 458 nm. The wavelength used for the 3.5 nm clusters was 514 nm. Low temperatures were achieved using a closed cycle helium cryostat.

XRD Measurements. X-ray powder investigations were carried out at room temperature with a STOE STADI P diffractometer (Cu $K\alpha_1$ radiation, $\lambda = 1.5406$ Å). Powders, obtained by scraping CdSe layers out the glass substrates, were glued on a steel sample holder and measured in reflection geometry (Bragg-Brentano). The time required for one measurement was 11 h.

HRTEM Measurements. High-resolution electron microscopic measurements were performed on a 120 kV Phillips CM 12 microscope equipped with a super-twin lens (Cs = 1.2 mm) and a 9800 EDX analyzer. For these investigations, the film samples were scraped away from the glass slides, wetted with a small amount of ethanol, placed onto a carbon-coated gold mesh grid, and transferred in an air-free holder into the microscope.

Results and Discussion

Structural Characterization of CdSe Clusters. In this paper, results from investigations on three different CdSe crystal sizes will be presented, prepared via the synthesis procedure depicted in Figure 1, and assigned as sample A (gyration size = 1.6 nm), sample B (= 3.0 nm), and sample C (= 3.5 nm quantum dots). Figure 3 depicts a typical high-resolution transmission electron micrograph of the sample B. One recognizes a very well-resolved ultrastructure of the single CdSe particles. We evaluated several microscopic images and could clearly identify that the CdSe nanocrystals, produced under our synthesis conditions, do not exhibit a spherical, but rather a triangular, shape (tetrahedral in 3D space). However, in Figure 3, the present not perfectly ordered particles are shown by different projection. That means the view on the pyramids is along different crystallographic directions. Additionally, some of the CdSe particles are aggregated. From the different projection and other micrographs in the tilted position, 3-dimensional structures can be calculated, which will be the subject of a future publication. The inset power spectrum displays a typical lattice structure reflecting the presence of the cubic zinc blende phase. The crystal size determination has been performed by counting the number of lattice planes, clearly seen in the HRTEM images. We recognized approximately 8−9 lattice planes at the projection 111 and 14−15 at the projection 220. That corresponds to an average size of 3.0 ± 0.2 nm. In the corresponding EDAX spectrum, X-ray fluorescence of Cd and Se has been detected. The average atomic Cd:Se ratio was determined on approximately 15 nm large spots to be 2:1, which coincides with the stoichiometry employed in the CdSe synthesis.

The nanocrystallinity of the samples used in this study is also demonstrated in Figure 4, showing experimental and calculated XRD patterns of two different CdSe quantum dot sizes (1.6 nm, upper part; 3.0 nm, lower part), taken with AMEO-ordered films. Although the reflections in the displayed patterns are strongly broadened, the theoretical cubic zinc blende patterns match the experimental data of the 3.0 nm crystallites much better than the hexagonal wurtzite diagrams. The XRD data of the 3.5 nm zinc blende crystals (not shown in the figure) do not differ significantly from that of the 3.0 nm crystals. Furthermore, the XRD pattern of the extremely small 1.6 nm clusters corresponds neither to a cubic nor to a hexagonal phase.

Optical Absorption and Photostability of CdSe Clusters in Sols and Layers. As presented in the Experimental Section, we have developed two film preparation routes based either on direct coatings using highly concentrated CdSe sols or on the selenium infiltration into Cd-containing organosilicate gel layers. In accompanying optical absorption measurements we investigated the spectral shape of the lowest electronic transition in differently sized CdSe dot layers from both routes. The results of these studies are summarized in Figure 5. One recognizes the size quantization-controlled HOMO-LUMO features located at 410 nm (A, 1.6 nm clusters), at 520 nm (B, 3.0 nm nanocrystals), and at 560 nm (C, 3.5 nm dots) in the optical spectra of the films prepared from 0.5 M AMEO stabilized sols (Figure 5a). The quite pronounced spectral shape of these lowest absorption features shows that the cadmium ethoxy

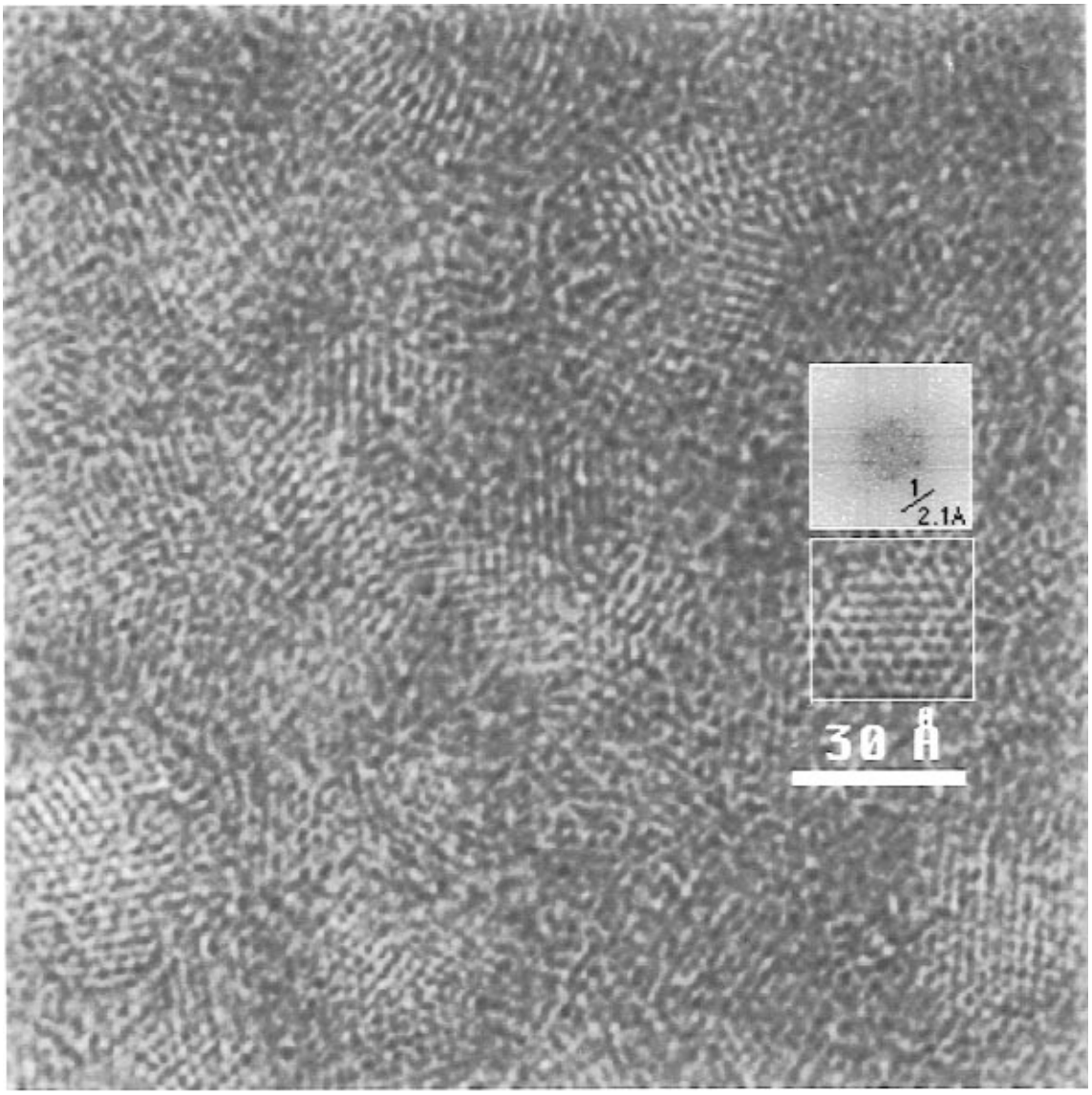

Figure 3. HRTEM image of 3.0 nm CdSe nanocrystals. Inset: the corresponding power spectrum reflects the presence of a cubic zinc blende phase.

acetates and AMEO are powerful precursors for the synthesis of narrowly sized colloids and layers on glass supports. One might sharpen the size distribution of the larger nanocrystals using size selective precipitation that is currently under study. The volume fraction of the CdSe particles in the resulting films is fairly high, approaching nearly 5%. The above highly concentrated colloids could also be diluted with prehydrolyzed organosilicate sols to form composite layers of variable CdSe volume fraction without noticeable changes in the optical spectra.

On the other hand, the organosilicate-based preparation, where a selenium source infiltration takes place, resulted in a non-structured absorption tail between 350 and 500 nm (Figure 5b). Under these conditions, poorly defined clusters are formed along the polymeric chains of the matrix containing statistically distributed cadmium ions. With increasing curing temperature up to 250 °C, the initial yellow CdSe films with clusters smaller than 2 nm turned to orange-red due to the aggregation to larger 3−4 nm nanocrystals, also to be recognized on the observed red shift in the optical absorption spectrum. The accompanying occurrence of weakly pronounced absorption bumps at 410, 480, and 540 nm reflects a strong matrix related hindrance of sharpening the nanocrystal size distribution. Apparently, the matrix stiffening via organic polyaddition reactions taking place during the thermal curing produces nonuniform pore structures, avoiding development of symmetrically well-defined larger nanocrystals. By comparing the spectral shapes produced by these two routes, we can conclude that one can better control the sharpness of the excitonic bands by choosing an appropriate chemical synthesis of the nanocrystals prior to coatings. The results of these systematic CdSe synthesis optimizations will be published in more detail elsewhere.[18] An additional advantage of the above presented single-step-coating procedures is the broadly adjustable thickness up to 10 μm that allows to employ these highly transparent crack-free films as wave guides.

The conversion of the sols into transparent films significantly enhances the quantum dot photostability. This has been checked in steady-state irradiations of the sols and films using polychromatic light of a 500 W Hg−Xe lamp. The results of this study are shown in Figure 6, reflecting changes in optical absorption spectrum of an air-saturated AMEO-stabilized CdSe colloid in ethanol with increasing irradiation time. After 80 min of irradiation, the intensity of the 410 nm absorption feature dropped to 20% of its initial value due to the photoanodic cluster dissolution, well-known from earlier studies.[19] The inset with the normalized optical density at 410 nm plotted versus the

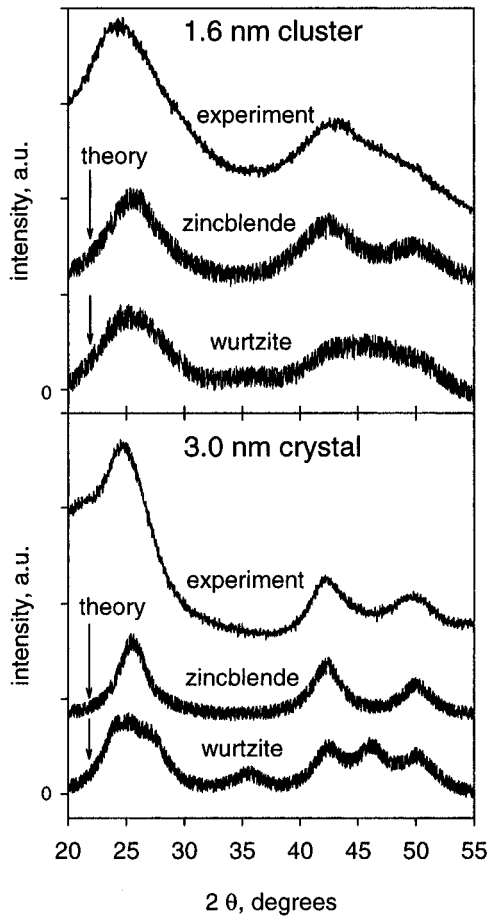

Figure 4. Experimental and theoretical (for zinc blende and wurtzite) X-ray diffraction patterns of CdSe nanocrystals: upper part, 1.6 nm clusters; lower part, 3.0 nm particles.

irradiation time indicates that the CdSe clusters embedded in organosilicates (network modified with alumina (b) or titania (c)) are more stable than in air-saturated ethanol (a).

The demonstrated photostability indicates that the organosilicate matrix is an efficient oxygen diffusion barrier. (Oxygen is known to be responsible for the photoanodic dissolution of semiconductor nanoparticles.[19]) Why the alumina-containing layers show stronger photodecomposition (b) in comparison to titania-containing organosilicate samples (c) is not clear at present (Figure 6). One possible explanation might be a significantly lower alumina content used in the lacquer synthesis, resulting in more open porous structures with higher oxygen permeability. Furthermore, we also tested the photostability of AMEO-ordered CdSe films exhibiting an excellent photostability after 1 day of continuous UV irradiation. However, it is of note that the nanocrystal concentration in coating sols, molar AMEO/Cd ratio, and the adjustment of the thermal curing conditions strongly determine the resulting photostability.

Steady-State Photoluminescence. The above-presented AMEO-ordered CdSe layers with pyramidal dots are strongly fluorescing with a quantum yield nearly 10% at room temperature. This allows to employ photoluminescence excitation spectroscopy to visualize several "magic" electronic transitions in these nanocrystals, not resolvable in optical absorption measurements. At this point, we refer the reader to reports dealing with the optical spectroscopy of magic clusters in ellipsoidal[20] and spherical[21] wurtzite CdSe systems or in other II−VI nanocolloids,[1] quantum dot gels, and crystals.[22]

Figure 7 depicts our results (excitation and emission spectra) collected on coating CdSe sols and the subsequently prepared

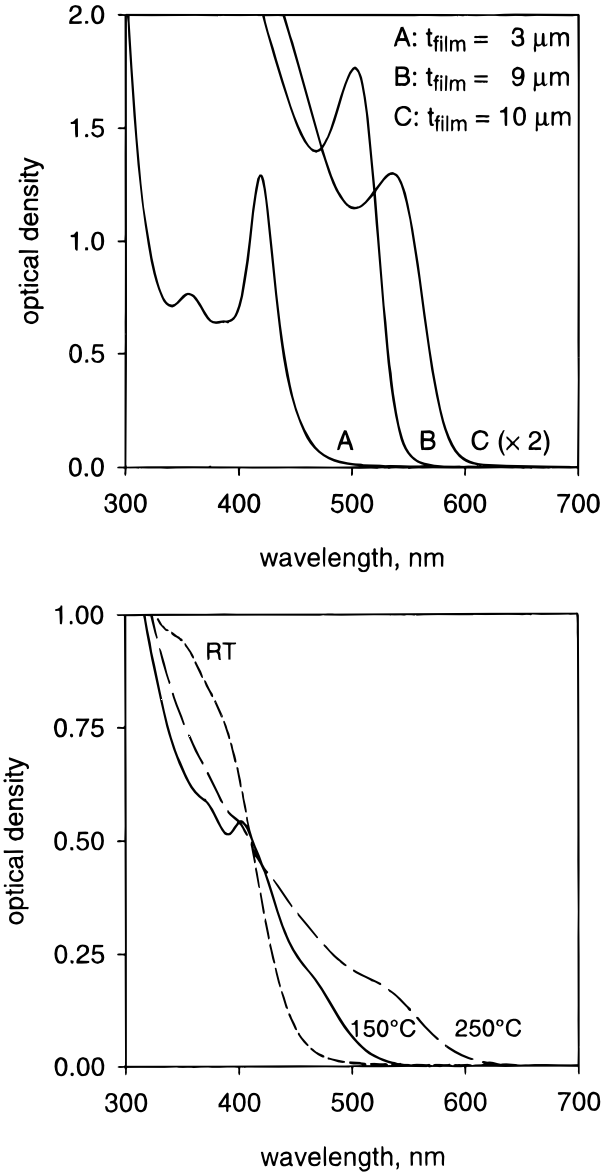

Figure 5. Optical absorption spectra of differently synthesized CdSe films. (a, top) AMEO-ordered thick layers of different thickness t_{film} and crystal size (A, 1.6 nm; B, 3.0 nm; C, 3.5 nm crystallites). (b, bottom) Thermal growth of CdSe in organosilicate-ordered layers, thickness 6 μm (for details see text below).

films composed of 1.6 (A), 3.0 (B), and 3.5 nm quantum dots (C). It is clearly seen that, by thermal heating of the initial clusters A in 2-butoxyethanol or in 2-phenoxyethanol to yield larger crystals B and C, the initially broad and strongly Stokes-shifted emission spectrum converts into a narrower band located close to the lowest excitation level. Additionally, by converting the coating sols into the films, the excitation spectra exhibit additional red-shifted transitions at 470 nm (sample A) and at 520 nm (sample B), indicating a cluster−cluster aggregation, taking place during the thermal film curing in vacuum. Similarly interpreted spectroscopic observations were made in previous cluster consolidation studies on highly concentrated ZnO colloids and gels.[22a]

By comparing the excitation spectra of the films, one additionally recognizes that the excitation transitions at 350, 400, and 470 nm, contributing to the light emission in initial clusters A, are also contributing to the band edge photoluminescence in larger quantum dots B and C. This reflects not only an enormous stability of the initial 1.6 nm clusters, but it also deserves an additional discussion of the excitation−

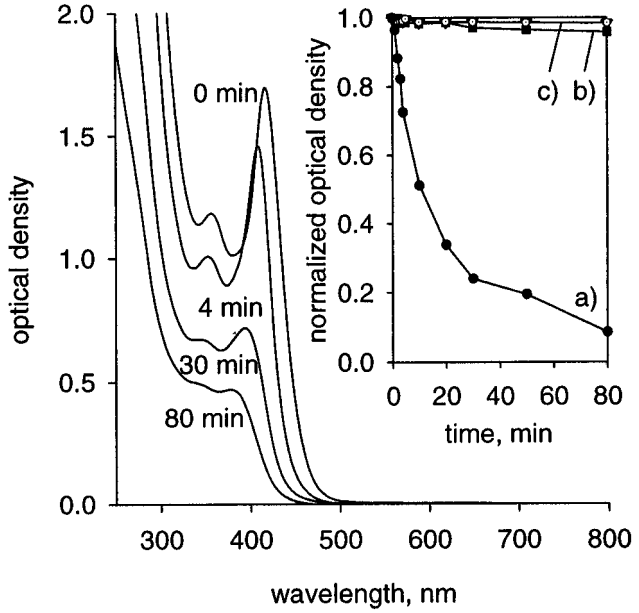

Figure 6. Changes in the optical absorption spectrum of an ethanolic AMEO-stabilized CdSe colloid exposed to UV light from a 500 W Hg−Xe high-pressure lamp under ambient air conditions. Inset: photoanodic dissolution rate in ethanolic colloid expressed in terms of optical density changes at 400 nm with increasing irradiation time (a); for comparison, optical density changes of the corresponding organosilicate films containing either alumina (b) or titania (c) are also included (see also text further below).

recombination mechanism, for which several possibilities exist. For example, the four dominant electronic transitions in the spectrum of the film sample C could be interpreted in terms of an excitation into the first and higher excitonic states inside of one quantum dot. This would mean that the same energetic position of these transitions in the initial small clusters A is purely accidental.

A more realistic view is to start from a broad size distribution within the film sample, where a short-range exciton tunneling from smaller clusters (of larger band gap) into the neighboring larger quantum dots B or C (of smaller band gap) could occur. In addition, a long-range electronic energy transfer between a small cluster A (donor) and a larger quantum dot B or C (acceptors) over distances of a few cluster diameters should be also taken into account (dipole−dipole interaction). However, our HRTEM images of the 3.0−3.5 nm crystals do not indicate the presence of the initial precursor clusters A, previously annealed for several hours at 150−300 °C.

Thus, another possible explanation arises, in our view a highly probable one, defining the 3.0−3.5 nm CdSe crystallites in sols and in films not as fully dense solid objects, but rather as complex nanoporous moieties. They would be the result of quantized cluster−cluster aggregations producing dots with primary, secondary, tertiary, etc., pore sizes responsible for the existence of strongly localized excitonic transitions within one quantum dot (multiple cluster−cluster aggregate). With this argument one could understand why all the magic transitions seen in Figure 7 contribute to the band edge emission at 580 nm. Interestingly, the growth of tetrahedral CdSe quantum dots starts with the appearance of two magic clusters smaller than 1 nm exhibiting sharp HOMO−LUMO features at 280 nm (molecular initiator cluster) and 350 nm (primary aggregate) as we have found in previous studies.[18] Hence, the 350 nm peak in the above-displayed excitation spectra is not a higher order transition, but rather a strongly localized HOMO−LUMO transition within a multiple 3.5 nm cluster−cluster aggregate. Nevertheless, more thorough future HRTEM and SAXS investigations are needed to verify the above-proposed multiple aggregate structures.

Time-Resolved Photoluminescence. As the small CdSe nanocrystallites discussed in this paper are characterized by a large surface/volume ratio, the question of intrinsic or surface-related recombination mechanisms arises. In order to analyze

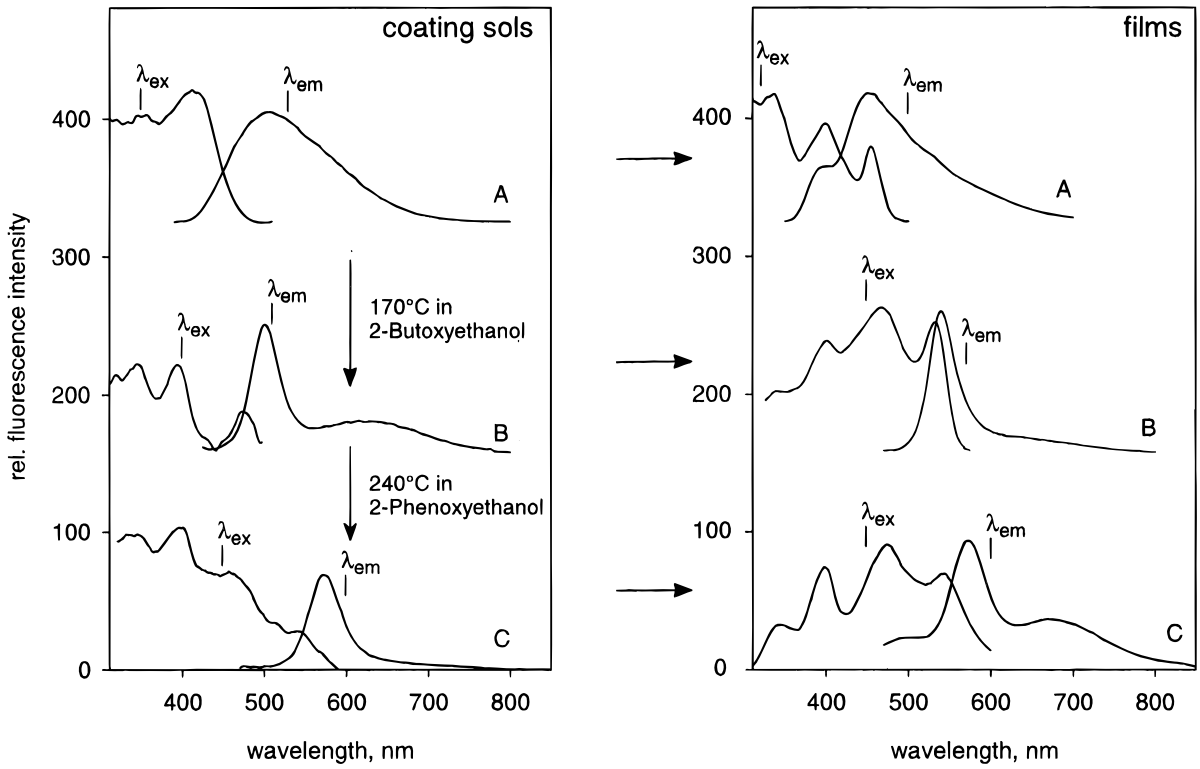

Figure 7. Fluorescence excitation and emission spectra of the CdSe coating sols and the corresponding AMEO-ordered CdSe layers containing 1.6 (A), 3.0 (B), and 3.5 nm (C) crystallites. The excitation spectra are corrected for the emission background of the excitation lamp.

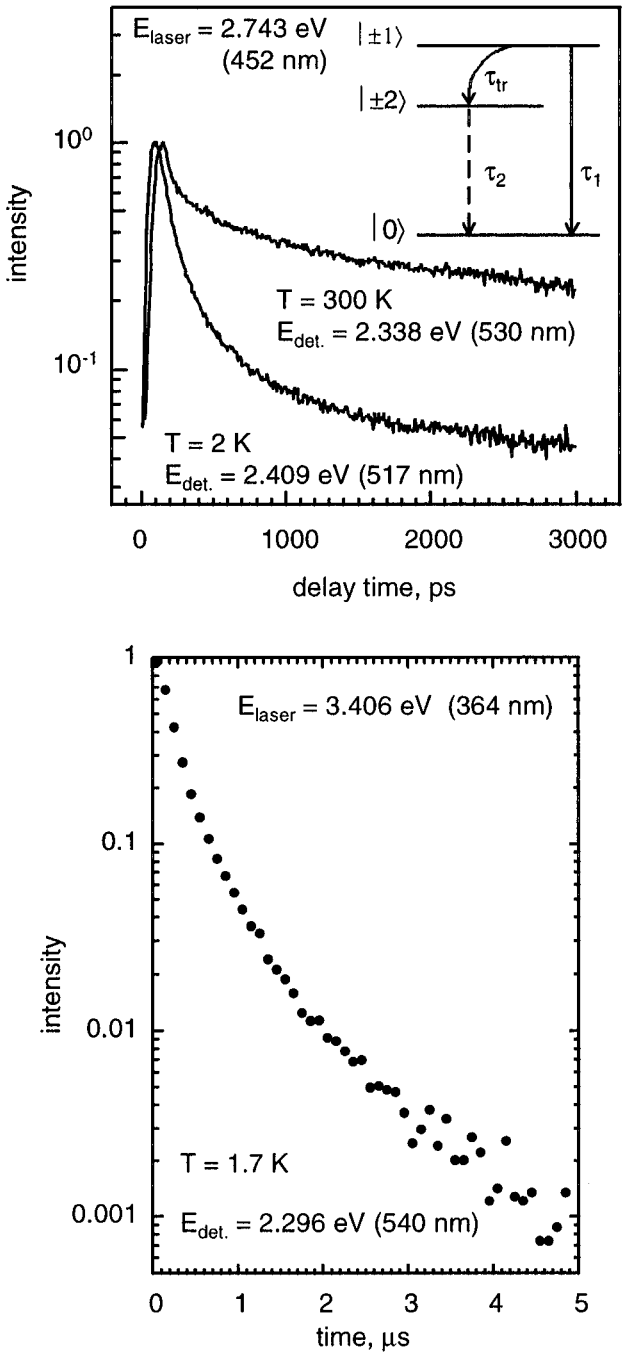

Figure 8. (a, top) Decay characteristics of the photoluminescence signal of 3.0 nm CdSe crystals at 300 and 2 K. The detection wavelength was set at the maximum of the PL signal. (b, bottom) Decay of the slow relaxing components (for details see text).

the carrier dynamics in nanocrystalline AMEO−CdSe films, temperature-dependent time-resolved PL measurements have been performed within the range between 1.7 and 300 K. As a model system, we investigated the film sample B composed of 3.0 nm quantum dots (for photoluminescence spectra see Figure 7). For these structures, the Stokes shift between the PL and the lowest absorption maximum is smaller than 50 meV.

Figure 8 shows the PL decay curves obtained with two different setups with a picosecond (part a) and a 100 ns time resolution (part b). The 9 μm thick film sample was excited at 452 nm in the picosecond and at 364 nm in the 100 ns experiment, i.e., on the high-energy side of the lowest optical absorption feature located at 520 nm at room temperature (see Figure 7). The detection wavelength has been adjusted to the maximum of the PL signal. In the picosecond experiment, a biexponential decay was observed represented by two time constants with values of about $\tau_{tr} = 100$ ps and $\tau_1 = 4.7$ ns, nearly independent of temperature between 2 and 300 K. However, the PL intensity ratio of the fast and slower recombination process decreases with increasing temperature. As depicted in Figure 8b, a slow multiexponential decay with time constants in the submicrosecond range at 1.7 K, vanishing rapidly for temperatures above 100 K, is observed in the 100 ns experiment.

To interpret the above experimental data, we suggest the following model idea.[7,23] Recently, published reports discuss that crystal fields and shape asymmetry of the nanocrystallites as well as an electron−hole exchange interaction might cause a splitting of the 8-fold degenerate ground state of the quantum dots[7,12,23] into four discrete levels within the valence band and two separate levels within the conduction band. Following this argumentation, the electronic transition from the first excited state (indicated in the inset of Figure 8a as $|\pm 2\rangle$) into the ground state (LUMO) is dipole-forbidden and related to the slow microsecond decay time constants. On the other hand, the dipole-allowed transition from the energetically higher lying valence band state (indicated in Figure 8a as $|\pm 1\rangle$ and separated typically several millielectronvolts from the ground state[23]) would then be attributed to the time constant $\tau_1 = 4.7$ ns. The fast $\tau_{tr} = 100$ ps process consequently characterizes the relaxation between these two dipole-allowed and -forbidden transitions. Of special interest is the above-noted temperature independence of the 4.7 ns process. In contrast to studies on two-dimensional quantum wells[24] or one-dimensional quantum wires,[25] where an increase of the carrier lifetime τ according to $\tau \propto T$ or $\tau \propto \sqrt{T}$, respectively, was observed, it seems that in completely confined zero-dimensional systems the lifetime of dipole-allowed transitions is independent of temperature.

In order to interpret the complex decay characteristics of the submicrosecond components, the role of surface photoredox chemistry and possible differences in the internal molecular structure, both strongly related to the chemical nature of molecular precursors and synthesis conditions employed as well as sample inhomogeneities,[7] have to be taken into account. Bawendi et al.,[7,9,12] who reported similar time decay data collected on TOPO-capped CdSe quantum dots, discuss an additional role of surface states serving as traps for the holes. The role of surface states is also underlined in the most recent report on CdSe-containing borosilicate glasses, where a non-exponential decay in the microsecond range was observed,[26] attributed to charge carriers traps, where the nature and energy of those states are determined by the way how the surface atoms are bound to the surrounding matrix.

In our AMEO-ordered CdSe layers, we deal with a highly complex surface chemistry (see Experimental Section). The FTIR and chemical analysis data collected on thermally cured film samples indicate the presence of acetates, OH groups, and amine ligands bound to the cadmium-terminated CdSe surface (Cd/Se ratio = 2). Thus, there are several possibilities to produce shallowly trapped holes (chemically speaking to generate oxygen-, nitrogen-, and selenium-centered radical anions) and electrons (metal vacancies due to Cd-enriched cluster surface) after the light absorption. However, to clarify the correlation between such effects and the submicrosecond time constants observed in the experiment more quantitatively, further studies are required.

Resonance Raman Investigations on CdSe Films. The Raman spectra of the AMEO-capped CdSe layers A, B, and C (for optical spectra see Figures 5a and 7) recorded at 10 K are shown in Figure 9. One recognizes an intense photolumines-

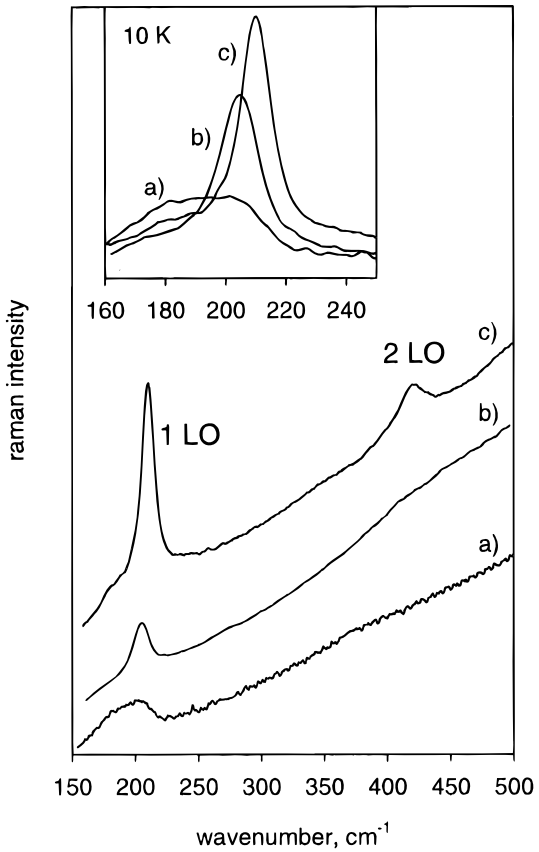

Figure 9. Raman spectra collected at 10 K on AMEO-ordered CdSe layers of different crystal sizes: 1.6 (a), 3.0 (b), and 3.5 nm (c). The inset shows the same spectra in the vicinity of the 1LO phonon band of CdSe; here the spectra are corrected for the luminescence background.

TABLE 1: Band Gap Energy E_g, 1LO Phonon Wavenumber ν_{LO}, and Line Width (fwhm) of the 1LO Phonon for Three Different CdSe Nanocrystallites

R (nm)	E_g (eV)	ν_{LO} (cm^{-1})	fwhm (cm^{-1})
1.75	2.21	210	10.6
1.5	2.38	206	14.8
0.8	3.02	204.5	22.8

cence background caused by radiative recombination discussed in the previous chapters. All spectra show a well-resolved vibrational mode at about 207 cm^{-1}, which is close to the 1LO phonon of the CdSe bulk material (210 cm^{-1}). Therefore, we conclude that the observed Raman signal is due to the CdSe lattice vibration.

For the 1.6 and 3.0 nm clusters the Raman intensity is very weak compared with the luminescence background (Figure 9a,b). Regarding the Raman band corresponding to the 1LO phonon, we noticed an increase of the 1LO phonon line width with decreasing cluster size (Table 1). This size-dependent broadening of the LO phonon can be clearly seen in the inset of Figure 9, which shows the LO phonon peak of the three samples corrected for the fluorescence background. We also observe that the LO phonon frequency shifts to lower values with decreasing CdSe crystal size (Table 1).

In the literature only theoretical treatments of the size-dependent phonon frequency shift are reported.[13,14,16] Shiang and co-workers[13] have suggested a theoretical model concerned with the phonon confinement in CdS nanocrystallites that predicts a considerable shift of the LO frequency to lower energies as well as an asymmetrical broadening of the LO band for decreasing crystallite sizes. The applied model is based on the vibrational multimode nature for lattices with finite sizes. While the predicted broadening was observed in their experiments, they found only a very small red shift of the LO frequency. In order to explain their experimental results, a second effect changing the phonon line position was considered. They assumed a blue shift caused by strain acting on the surface of the nanocrystallites. These two contrary effects were suggested to cancel each other.

In our experiments, we observed a red shift of about 6 cm^{-1} as the cluster size decreases from 3.5 to 1.6 nm. Although this shift is still smaller than the one predicted by the theory, the increasing influence of the contribution correlated with the phonon confinement becomes evident.

In the Raman spectra (Figure 9) we observe an additional shoulder on the low wavenumber side of the LO phonon. The intensity of the shoulder gains in significance as the cluster size decreases. The shoulder can be explained if one takes into account the growing influence of the surface for very small nanocrystallites. For the three samples investigated in our experiments, the surface-to-volume ratio, in the classical view of a fully dense spherical object, is very high, calculated to be 93, 68, and 61% for the 1.6, 3.0, and 3.5 nm crystals, respectively.

Klein et al.[13c] have reported on surface optical modes which they observed in their Raman spectra, as a wing on the low-frequency side of the LO phonon. They have calculated the frequencies of these surface modes for CdSe dots embedded in a glass matrix and found values ranging from 194 to 200 cm^{-1}.

However, surface optical modes are forbidden in the case of spherically shaped nanocrystallites since the lowest order surface modes do not couple to the spherically symmetric charge distribution of a $1S_e-1S_h$ type wave function. This leads to the conclusion that the shape of the cluster under investigation differs from that of a sphere, which is in accordance with our results obtained from HRTEM investigations. For the 1.6 nm clusters a considerable contribution of surface modes can be expected as nearly all atoms are located on the cluster surface.

Summary and Outlook

In this quantum crystallite study, concerned with the development and basic spectroscopy of photonic II−VI semiconductor films on glass supports, the feasibility of sol−gel processing was again demonstrated. CdSe volume fractions of nearly 5% and highly transparent films with thicknesses of nearly 10 μm were achieved. The presented photoluminescence decay data interpreted in terms of a ground-state splitting and existing shallow surface traps confirm the earlier experimental and theoretical observations made by other groups on quantum dot samples with completely different precursor chemistry and environment. The firstly demonstrated significant red shift and line broadening of the LO phonon in Raman spectra allowed not only to specify the upper size limit of about 3.5 nm, above which the LO phonon frequency becomes size invariant, but also to highlight the addressed structural aspects accompanying all chapters of this paper. In the vicinity and below 3.5 nm, our strongly nonstoichiometric CdSe quantum dots manifest new, previously not evaluated internal structures.

Acknowledgment. We gratefully acknowledge financial suppport from the Deutsche Forschungsgemeinschaft (Sonderforschungsbereich 410) and from the Fonds der Chemischen Industrie. T.B. was supported by the Graduiertenkolleg "Mikrostrukturierte Halbleiter".

References and Notes

(1) For recent reviews see: (a) Flytzanis, C.; Hache, F.; Klein, M. C.; Ricard, D.; Roussignol, Ph. *Prog. Opt.* **1991**, *29*, 323. (b) Banyai, L.; Koch,

S. W. In *Series on Atomic, Molecular and Optical Physics*; World Scientific Publishing Co.: Singapore, 1993; Vol. 2. (c) Weller, H. *Angew. Chem., Int. Ed. Engl.* **1993**, *32*, 41. (d) Brus, L. E. *J. Phys. Chem.* **1994**, *98*, 3577. (e) Henglein, A. *Ber. Bunsen-Ges. Phys. Chem.* **1995**, *99*, 903. (f) Wang, Y. *Adv. Photochem.* **1995**, *19*, 179. (g) Woggon, U.; Gaponenko, S. V. *Phys. Status Solid: B* **1995**, *189*, 285. (h) Alivisatos, A. P. *Science* **1996**, *271*, 933.

(2) (a) O'Regan, B.; Moser, J.; Anderson, M.; Grätzel, M. *J. Phys. Chem.* **1990**, *94*, 8720. (b) Hotchandani, S.; Kamat, P. *J. Phys. Chem.* **1992**, *96*, 6834. (c) Hoyer, P.; Eichberger, R.; Weller, H. *Ber. Bunsen-Ges. Phys. Chem.* **1993**, *97*, 630. (d) Hotchandani, S.; Das, S.; Thomas, K. G.; George, M. V.; Kamat, V. P. *Res. Chem. Intermed.* **1994**, *20*, 927. (e) Kamat, P. V. *Prog. Inorg. Chem.* **1997**, *44*, 273.

(3) (a) Wang, Y. *Nature* **1992**, *356*, 585. (b) Wang, Y.; West, R.; Yuan, C. H. *J. Am. Chem. Soc.* **1993**, *115*, 3844.

(4) (a) Colvin, V. L.; Schlamp, M. C.; Alivisatos, A. P. *Nature* **1994**, *370*, 354. (b) Dabboussi, B. O.; Bawendi, M. G.; Onitsuka, O.; Rubner, M. F. *Appl. Phys. Lett.* **1995**, *66*, 1316.

(5) (a) Spanhel, L.; Arpac, E.; Schmidt, H. *J. Non-Cryst. Solids* **1992**, *147&148*, 657. (b) Choi, K. M.; Shea, K. J. *J. Phys. Chem.* **1994**, *98*, 3207. (c) Spanhel, L.; Popall, M.; Müller, G. *Proc. Indian Acad. Sci. (Chem. Sci.)* **1995**, *107*, 637.

(6) (a) Hof, M.; Schleicher, J.; Schneider, F. W. *Ber. Bunsen-Ges. Phys. Chem.* **1989**, *93*, 1377; (b) **1993**, *97*, 172.

(7) Nirmal, M.; Norris, D. J.; Kuno, M.; Bawendi, M. G.; Efros, Al. L.; Rosen, M. *Phys. Rev. Lett.* **1995**, *75*, 3728.

(8) Shum, K.; Tang, G. C.; Junnarkar, M. R.; Alfano, R. R. *Appl. Phys. Lett.* **1987**, *51*, 1839.

(9) Bawendi, M. G.; Carroll, P. J.; Wilson, W. L.; Brus, L. E. *J. Chem. Phys.* **1992**, *96*, 946.

(10) Ghanassi, M.; Schanne-Klein, M. C.; Hache, F.; Ekimov, A. I.; Ricard, D.; Flytzanis, C. *Appl. Phys. Lett.* **1993**, *62*, 78.

(11) Nirmal, M.; Murray, C. B.; Bawendi, M. G. *Phys. Rev. B* **1994**, *50*, 2293.

(12) Efros, Al. L.; Rosen, M.; Kuno, M.; Nirmal, M.; Norris, D. J.; Bawendi, M. G. *Phys. Rev. B* **1996**, *54*, 4843.

(13) (a) Papavassiliou, G. C. *J. Mol. Struct.* **1982**, *79*, 395. (b) Rosseti, R.; Nakahara, S.; Brus, L. E. *J. Chem. Phys.* **1983**, *79*, 1086. (c) Klein, M. C.; Hache, F.; Ricard, D.; Flytzanis, C. *Phys. Rev. B.* **1990**, *42*, 11123. (d) Shiang, J. J.; Risbud, S. H.; Alivisatos, A. P. *J. Chem. Phys.* **1993**, *98*, 8433.

(14) Roca, E.; Trallero-Giner, C.; Cardona, M. *Phys. Rev. B* **1994**, *49*, 13704.

(15) Sood, A. K.; Menendez, J.; Cardona, M.; Ploog, K. *Phys. Rev. Lett.* **1985**, *54*, 2111.

(16) Lankers, M.; Göttges, D.; Materny, A.; Schaschek, K.; Kiefer, W. *Appl. Spectrosc.* **1992**, *46*, 1331.

(17) Deckert, V.; Kiefer, W. *Appl. Spectrosc.* **1992**, *46*, 322.

(18) Ptatschek, V.; Schmidt, T.; Lerch, M.; Müller, G.; Emmerling, A.; Fricke, J.; Foitzik, A. H.; Lange, B.; Spanhel, L. *Ber. Bunsen-Ges. Phys. Chem.*, in press.

(19) Henglein, A.; Gutierrez, M. *Ber. Bunsen-Ges. Phys. Chem.* **1983**, *87*, 852.

(20) Murray, C. B.; Norris, D. J.; Bawendi, M. G. *J. Am. Chem. Soc.* **1993**, *115*, 8706.

(21) Katari, J. E. B.; Colvin, V. L.; Alivisatos, A. P. *J. Phys. Chem.* **1994**, *98*, 4109.

(22) (a) Spanhel, L.; Anderson, M. A. *J. Am. Chem. Soc.* **1991**, *113*, 2826. (b) Murray, C. B.; Kagan, C. R.; Bawendi, M. G. *Science* **1995**, *270*, 1335. (c) Vossmeyer, T.; Reck, G.; Katsikas, L.; Haupt, E. T. K.; Schulz, B.; Weller, H. *Science* **1995**, *267*, 1476.

(23) Woggon, U.; Gindele, F.; Wind, O.; Klingshirn, C. *Phys. Rev. B* **1996**, *54*, 1506.

(24) Feldmann, J.; Peter, G.; Göbel, E. O.; Dawson, P.; Moore, K.; Foxon, C.; Elliot, R. J. *Phys. Rev. Lett.* **1987**, *59*, 2337.

(25) Kono, T.; Tsukamoto, S.; Nagamune, Y.; Sogawa, F.; Nishioka, M.; Arakawa, Y. *Appl. Phys. Lett.* **1994**, *64*, 1564.

(26) Jungnickel, V.; Henneberger, F. *J. Lumin.* **1996**, *70*, 238.